Measuring the Faraday effect in olive oil using permanent magnets and Malus' law

Daniel L Carr, Nicholas L R Spong, Ifan G Hughes and Charles S Adams

Joint Quantum Centre (JQC) Durham–Newcastle, Department of Physics, Durham University, South Road, Durham, DH1 3LE, United Kingdom

E-mail: daniel.l.carr@durham.ac.uk

Abstract. We present a simple permanent magnet set-up that can be used to measure the Faraday effect in gases, liquids and solids. By fitting the transmission curve as a function of polarizer angle (Malus' law) we average over short-term fluctuations in the laser power and can extract phase shifts as small as $\pm$ 50 μrads. We have focused on measuring the Faraday effect in olive oil and find a Verdet coefficient of $V = 192 \pm 1$ deg T^{-1} m^{-1} at approximately 20 °C for a wavelength of 659.2 nm. We show that the Verdet coefficient can be fit with a Drude-like dispersion law $A/(\lambda^2 - \lambda_0^2)$ with coefficients $A = 7.9 \pm 0.2 \times 10^7$ deg T^{-1} m^{-1} nm^2 and $\lambda_0 = 142 \pm 13$ nm.

Keywords: Faraday effect, Verdet coefficient, Malus' law, olive oil

1. Introduction

The Faraday effect (see e.g. [1]) has a wide range of applications including filtering [2, 3] and limiting feedback in optical systems [4]; it also affects light propagating through interstellar media [5]. The effect occurs when a magnetic field parallel to the direction of light propagation induces a circular birefringence in a medium which causes linearly polarized light to rotate as it travels through the medium. The magnitude of this rotation (θ) may be expressed as $\theta = VBl$, where B is the magnetic field strength, l the path length and V is a material-dependent factor known as the Verdet coefficient [1].

Studying the Faraday effect (see e.g. [6, 7]) and other examples of circular birefringence such as optical rotation in sugar solutions [8, 9, 10] is a common experiment in undergraduate teaching labs, as it elegantly links the concepts of polarization, dichroism, birefrigence and scattering [1]. However, measuring the Faraday effect can be challenging, especially in cases where the Verdet coefficient is small or the optical path length is short. There are many different methods proposed in the literature, some utilizing DC fields [11, 12, 13, 14, 15] and some AC fields [16, 17, 18, 19, 20, 21, 22]; by modulating the field and using a lock-in amplifier it is possible to extract rotation angles in the range of microradians. Most experiments employ electromagnets producing fields typically in the range of up to 0.025 T [16, 21] although experiments with larger fields have been performed [12].

In this paper, we report on a simple Faraday measurement apparatus based on small permanent magnets where fields over 0.6 T are easily accessible. The experiment

is inexpensive as it does not require the use of an electromagnet or lock-in amplifier. We show that by fitting a Malus' law transmission curve it is possible to measure polarization rotations as small as 50 μrads without the need for field modulation. Consequently, the DC Faraday effect is observable even in weakly magneto-optical materials.

To demonstrate the capabilities of our apparatus, we have measured the Verdet coefficient of olive oil, which was of interest due to a suggestion in the literature of an anomalously high Verdet coefficient at 650 nm [23], contradicting more recent measurements [21]. Our measurements show that the Verdet coefficient of olive oil is similar to other liquids such as water and much smaller (about 2 rad T^{-1} m^{-1} at 780 nm) than Faraday active magneto-optical materials such as the crystal TGG (82 rad T^{-1} m^{-1}) and resonant media such as Rb vapour (1.4×10^3 rad T^{-1} m^{-1}) [4].

2. Theory

From Malus' law (see [1]) the optical power (P) of a of linearly polarized light passing through a polarizer is

$$P = P_0 \cos^2 \phi, \tag{1}$$

where P_0 is the incident power and ϕ is the angle of the polarizer relative to the polarization direction of the incident light. Light passing through a circularly birefringent medium has its plane of polarization rotated by an angle θ. When the optically active medium is placed between the polarizers, we may describe the light transmitted through the polarizers using

$$P = P_0 \cos^2(\phi + \theta) + c. \tag{2}$$

Here we have introduced an offset c to account for imperfect extinction of the polarizers and the presence of background light. It is worth noting that as the laser beam has a fixed size, the optical power is linearly proportional to the optical intensity (i.e. the power per unit area) by

$$I_0 = \frac{P_0}{\pi w_0^2/2}, \tag{3}$$

where I_0 is the incident intensity and w_0 is the laser beam radius. Therefore if desired it is possible to frame 1 and 2 in terms of optical intensity rather than optical power. The magnitude of rotation for a given magnetic field strength (B) and path length ($\mathrm{d}l$) is material-dependent and classified by the Verdet coefficient (V) such that

$$\theta = V \int_0^l B \mathrm{d}l = V B_{\mathrm{av}} l, \tag{4}$$

where B_{av} represents the average magnetic field strength across the sample and l is the sample's total length. Due to its relation to the material's refractive index [15], the Verdet coefficient is found to depend on the temperature and wavelength so may be modelled using a dispersion law. We tested this by determining the Verdet coefficient at multiple wavelengths and attempting to fit a dispersion curve. We compared the data to two separate models, the first being a Cauchy-type [24, 25] dispersion of the form

$$V(\lambda) = A + \frac{B}{\lambda^2}, \tag{5}$$

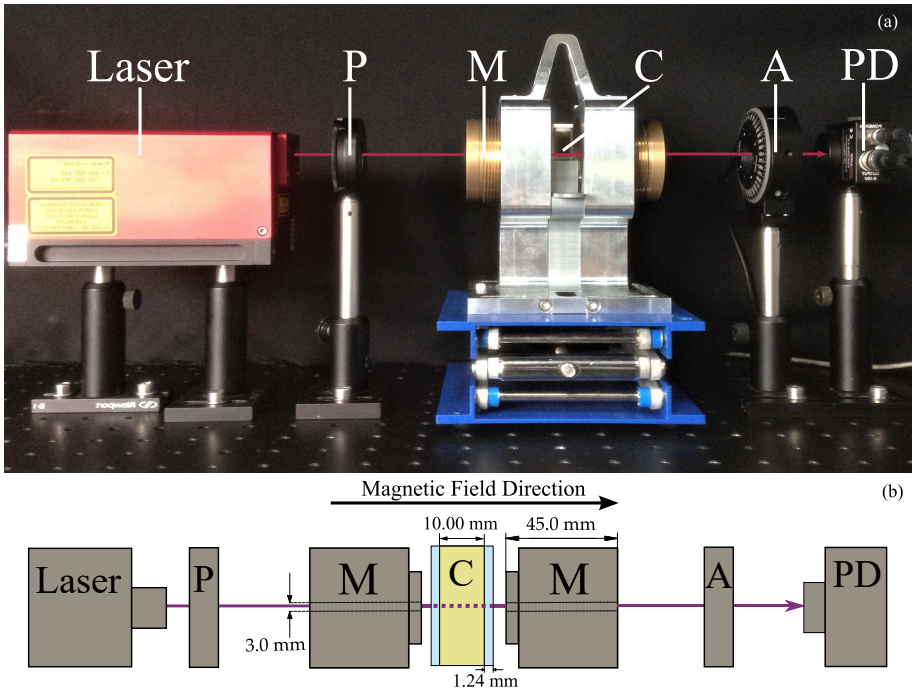

Figure 1. The arrangement of the apparatus. (a) A photograph of the equipment aligned on an optical breadboard. The arrow shows the direction of laser propagation. P = polarizer, M = permanent magnet, C = glass cuvette, A = analyzer, PD = photodiode. The analyzer and photodiode were both connected to a PC, which could automatically rotate the analyser and read voltages from the photodiode. (b) A schematic drawing displaying the dimensions of the annular magnets and the cuvette.

where A and B are both fitting parameters and λ is the wavelength of light. Secondly we attempted to fit a Drude-type [26] dispersion of the form:

$$V(\lambda) = \frac{A}{\lambda^2 - \lambda_0^2}, \tag{6}$$

where now A and λ_0 are the two fitting parameters. We believed using the Drude model would provide a more profound insight into the underlying physics as the value of λ_0 should correspond to an absorbance peak.

3. Methods

The experimental apparatus consisted of simple optical equipment, commonly available in an undergraduate laboratory. The arrangement of the equipment is shown in figure 1. Measurements of optical rotation as a function of the magnetic field strength were obtained at 7 different wavelengths (405.4 nm, 446.6 nm, 518.8 nm, 637.8 nm, 659.2 nm, 681.8 nm and 796.2 nm) using HEXA-BEAM lasers (Photonics Technologies). Five of the wavelengths were studied using one HEXA-BEAM laser. This device was then replaced by another HEXA-BEAM laser and the experiment

was realigned to study the final two wavelengths. The advantage of using the HEXA-BEAM lasers is - depending on the modules installed - up to six wavelengths may be studied using a single device, without the need for realignment.

Light from the laser passes through a linear polarizer to ensure it is fully polarized before entering the sample. Polarized light then passes through a glass cuvette (Thorlabs CV10 Q3500F) containing an olive oil sample (Tesco Olive Oil) inside a magnetic field, and then through to an analyzer which consists of a second polarizer mounted in a rotation stage (Thorlabs PRM1/MZ8). Finally, the light is incident on a photodiode (Thorlabs PDA100A-EC) which measures the transmitted optical power (P in (2)). The photodiode is connected to a data acquisition device (National Instruments USB-6008) so that the optical power may be measured automatically on a PC.

The magnetic field was provided by a pair of neodymium (NdFeB) magnets in an aluminium mount; a schematic view of the magnets may be seen in figure 1 (b). The magnetic field strength could be varied by changing the distance between the magnets. The threaded design of the magnet holders and mount allowed the separation to be adjusted by rotating the magnet holders. Using a Hall probe, the magnetic field was measured at various magnet separation distances to determine its spatial homogeneity. Further details of the construction of the mount for the magnets and the full magnetic field strength calibration may be found in Appendix A. The same magnets may be used in a wide range of different applications (see for example [27]).

The rotation stage and photodiode were connected to a PC so that the angle of the analyzer could be controlled and the optical power at the photodiode (P) could be measured automatically. A computer algorithm was programmed which rotated the analyzer in increments of one degree and then measured the optical power of the light using the photodiode. In this way, a mean power with a standard error was measured at each angle over a full 360 degree analyzer rotation. The data were then fitted using Malus' law, as described in (2). The major advantage of using computer-controlled apparatus was the rapid collection of data - a full 360 degree rotation cycle was collected in approximately 10 minutes.

Applying the Malus' law fit to the data, as demonstrated in figure 2, yielded a value of the rotation (θ). Many experiments in the literature will measure rotations by observing the power change at a fixed analyzer angle - often 45 degrees where the power change will be maximized. However, the residuals of figure 2 indicate that measurements performed at a single angle are sensitive to short-term changes in the incident power and the offset, caused by power fluctuations of the laser and changes in background levels of light. Our method of fitting the model to the full range of the data reduces this issue by fully parameterizing the amplitude and offset. Hence, we may extract rotations precisely, insensitive to random short-term power fluctuations which occur within a single measurement. However, a limitation of our method is that we cannot account for fluctuations over a larger timescale such as a long-term drift in the laser power or background light level. As such, care must still be taken to control these parameters whilst acquiring data.

For each sample being measured, three sets of data were taken at each magnetic field strength to obtain a mean rotation with a standard error. The field strength was then altered and the new value of θ was calculated using the same procedure. At each magnetic field strength, we compared the measured rotation to the rotation obtained at the minimum field strength (215.4 $\pm$ 1.4 mT). Here we introduce some new notation: $\Delta\theta = \theta - \theta_0$, where θ_0 is the rotation at the lowest field value and $\Delta\theta$

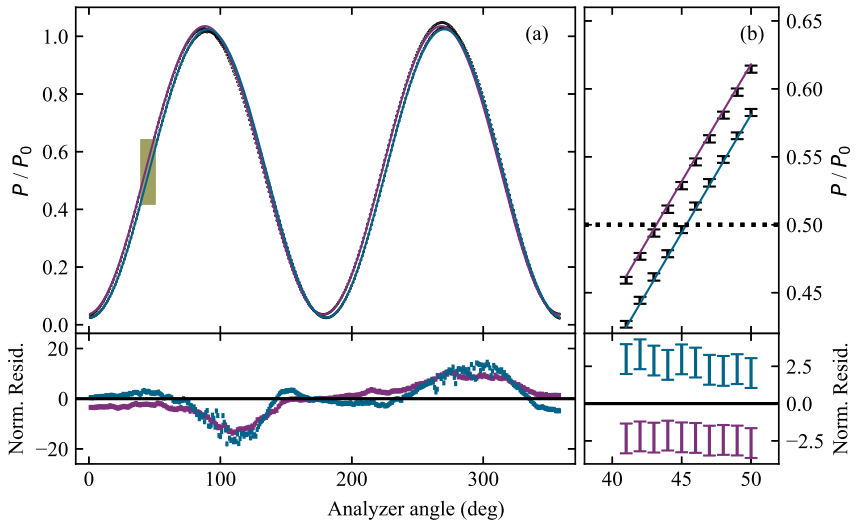

Figure 2. The phase shift for a "combined" sample (olive oil in a glass cuvette) at 446.6 nm. The solid lines are Malus' law models: $P = P_0 \cos^2(\phi + \theta) + c$ which have been normalized by the incident optical power (P_0). The left model (purple) is for data obtained at the minimum magnetic field strength (215.4 ± 1.4 mT) and the right model (blue) is for data obtained at the maximum magnetic field strength (618.8 ± 1.4 mT). The lower plots display the normalized residuals for the two different data sets. (a) Transmitted optical power as a function of analyzer rotation. The optical rotation is so small as to be almost imperceptible on this scale. (b) A zoom of the shaded area in (a) in which the offset c has been subtracted. A dotted line has been added to show the point of half maximum, the measurement point often used in the literature. The residuals show that even after offset subtraction, the data are still fluctuating in this region; hence the need for a rigorous fit to the entire data set (color online).

is the change in rotation. Ideally, the rotations would be compared to the sample in the absence of any field but this was not possible as the cuvette had to remain fixed in place during measurements due to the natural birefringence of the glass (this was achieved using a custom 3D-printed holder which slotted the cuvette in place inside the magnetic field). However, measuring from zero field would only introduce an offset to the measurements and not affect the gradient from which the Verdet coefficient is determined.

4. Results

Figure 2 shows example data that have been fit with a weighted least squares algorithm using the Malus' law method according to (2). For the data shown, the rotation change $\Delta\theta = 2.19 \pm 0.05$ degrees. This is one of the highest values that was observed and emphasizes the need for precise measurements.

When measuring the Verdet constant of olive oil, the glass cuvette in which the olive oil is contained also experiences the Faraday effect and so induces extra

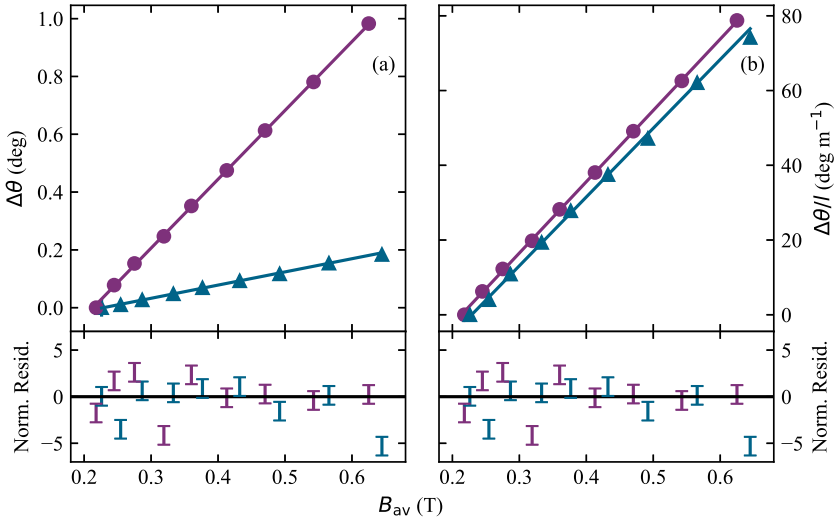

Figure 3. Comparison between the empty glass cuvette (triangles) and the "combined" measurement of the cuvette containing olive oil (circles) for a wavelength of 659.2 nm. (a) The rotation at each value of B_{av} for the two samples. This plot emphasizes that the rotation induced by the glass is large enough that it must be subtracted in order to study the rotation caused by the oil alone. (b) This plot displays the rotations normalized by length such that the gradient is the Verdet coefficient of the material. The Verdet coefficients for glass (see Appendix B) were found to be very similar to those of olive oil. Thus, $\Delta\theta_{\text{cuvette}}$ was only low due to the shorter path length of the glass.

optical rotation of the transmitted light. This may be seen in figure 3 where it is clear that the glass makes a significant contribution to the rotation. To account for this, measurements were made of the optical rotation due to the empty glass cuvette. The optical rotation due to the olive oil can then be calculated from a "combined" measurement of the optical rotation of the cuvette full of oil using

$$\Delta\theta_{\text{oil}} = \Delta\theta_{\text{combined}} - \Delta\theta_{\text{cuvette}}, \tag{7}$$

and so the Verdet coefficient may be determined using

$$V = \frac{\Delta\theta_{\text{oil}}}{B_{\text{oil}} l_{\text{oil}}}, \tag{8}$$

where B_{oil} is the average field strength experienced by the oil and l_{oil} is the path length of the oil. As this equation implies, a plot of $\Delta\theta_{\text{oil}}$ vs. B_{oil} allows the Verdet coefficient to be calculated by dividing the gradient by the path length.

As described in section 3, the Malus' law fitting procedure was repeated to obtain $\Delta\theta_{\text{oil}}$ values at each field strength such that a linear fit could be performed. The linear fits for 4 of the wavelengths are displayed in figure 4. Because there were errors in B_{oil} values and in $\Delta\theta_{\text{oil}}$, the data were fit using an orthogonal distance regression algorithm. The errors on the fitting parameters were obtained from the square roots of the relevant entries in the covariance matrix (procedure as outlined in [28]). The

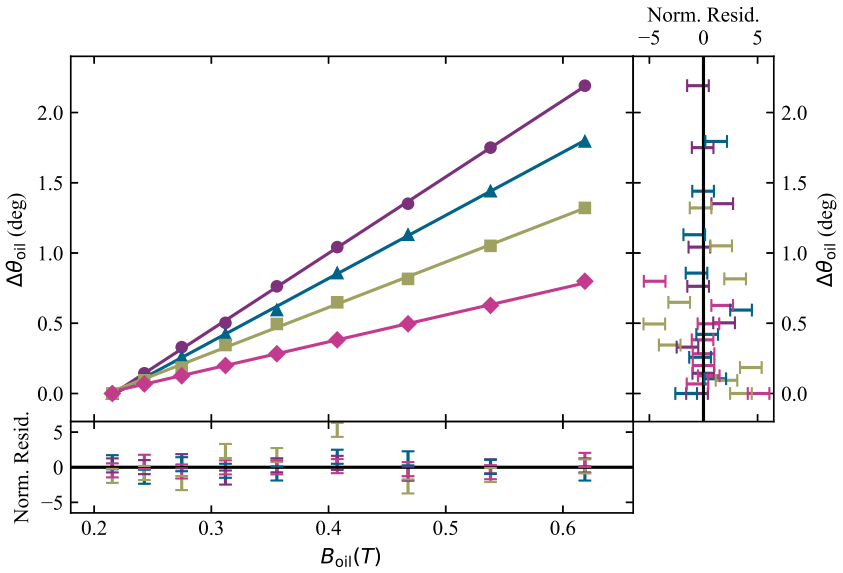

Figure 4. The change in rotation due to the oil ($\Delta\theta_{oil}$) for each magnetic field strength at 405.4 nm (circles), 446.6 nm (triangles), 518.8 nm (squares) and 659.2 nm (diamonds). Since $\Delta\theta_{oil} = VB_{oil}l_{oil}$ the data were fit with a straight line using orthogonal distance regression. Error bars are too small to be seen. The lower plot and upper right plot display the normalized residuals in the y direction and x direction respectively. Only 4 of the wavelengths are plotted to avoid too much overlapping of data points.

Table 1. The determined Verdet coefficients for olive oil at approximately 20 °C.

Wavelength ± 0.1 (nm)	Verdet coefficient (deg T^{-1} m^{-1})
405.4	543 ± 2
446.6	449 ± 2
518.8	323 ± 5
637.8	198 ± 2
659.2	192 ± 1
681.8	190 ± 10
796.2	146 ± 18

uncertainty in the Verdet constant was then propagated from the error in the gradient and the error in the path length. Table 1 gives the measured Verdet coefficients and uncertainties at each wavelength.

As shown in figure 5, the measured Verdet coefficients were fit with Cauchy-type and Drude-type dispersion curves using (5) and (6) respectively. For the Cauchy-type fit, the parameters were found to be A = -26 ± 4 deg T^{-1} m^{-1} and B = 9.42 ± 0.12 × 10^7 deg T^{-1} m^{-1} nm^2 while for the Drude-type fit they were A = 7.9 ± 0.2 × 10^7 deg T^{-1} m^{-1} nm^2 and λ_0 = 142 ± 13 nm. As before, the errors on these fitting parameters were obtained from the square root of the relevant entries in the covariance matrix.

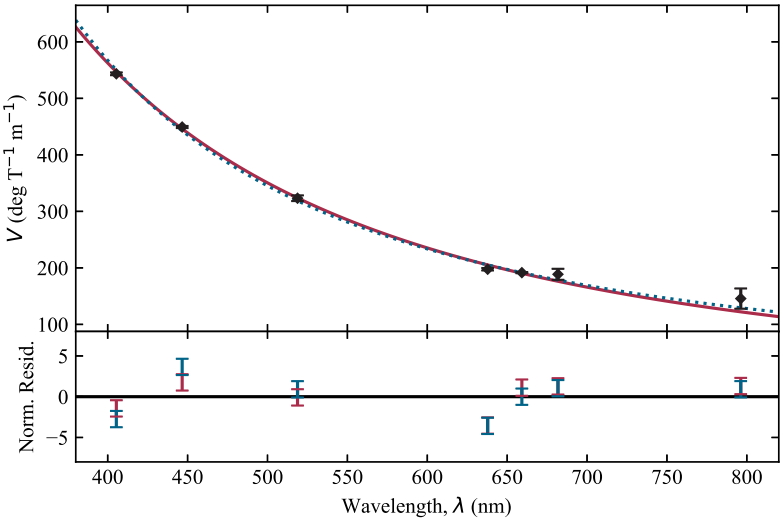

Figure 5. Dispersion plot for the variation of the Verdet coefficient of olive oil with wavelength at approximately 20 °C. Our data are represented by black diamonds with their error bars in the y direction displayed (error bars in x are too small to be seen). The solid red line represents the Cauchy-type model described by $V = A + B/\lambda^2$ and the dotted blue line represents the Drude-type model described by $V = A/(\lambda^2 - \lambda_0^2)$. The χ^2_ν values for these models are 4.45 and 7.28 respectively. The lower plot displays the normalized residuals.

5. Discussion

The dispersion relationship we determined is similar to that of other liquids such as water [16]. Our determined Verdet coefficients are also in good agreement with recent values present in the literature at similar wavelengths [21]. Similar to these recent measurements, we did not observe an anomalously high Verdet coefficient at 650 nm as was previously reported [23].

A restriction of using our permanent magnet set up is that much smaller path lengths must be used than, for example, in a solenoid set up. However, the high field strengths we were able to achieve help compensate for this and so measurable rotations are still easily observed. The path length of the oil was measured precisely using digital calipers so despite being small it did not introduce major uncertainty into the Verdet coefficient values.

We believe the major strength of our method is the rigorous Malus' law fitting which allows us to average over short-term random fluctuations in the laser power and detect rotations with errors on the order of tens of μrads. Performing the fit and allowing for an offset to be paramaterized makes the method insensitive to short-term fluctuations in the background level of light which are often difficult to control, particularly in a teaching laboratory. However, as discussed previously, our method is insufficient if there are significant long-term drifts in laser power or background light levels. If this were found to be a major issue, one possible way to eliminate it could be

to introduce a second photodiode to measure a blank background signal which may then be subtracted from the measured signal.

Traditionally, measuring the transmitted optical power over a full range of angles would be a tedious process, requiring manual rotation of the analyzer. Using the computer-controlled photodiode and analyzer makes the data collection much easier and faster. This means a Verdet coefficient may be determined even in a short laboratory session. The coding of the algorithm is also a vital skill as in modern physics laboratories data collection is becoming increasingly automated. The coding can either be partially or fully completed by students to give them an understanding of how the computer is interfacing with the equipment.

As shown in figure 2, the raw data give an excellent visual demonstration of Malus' law which students should be familiar with from earlier levels of teaching. Performing the fit provides students with a good opportunity to develop their model fitting and error analysis skills.

Experimental set-ups to study the Faraday effect are available commercially (see for example [29]). In comparison, our set-up based on permanent magnets, allows open access to the higher fields enabling the investigation of a wide range of weakly magneto-optical materials, including liquids. In addition, using the HEXA-BEAM laser, up to 6 wavelengths may be studied quickly rather than just one, making it easier to observe dispersion effects. Perhaps the greatest advantage of our set-up over commercial system is the automation using the rotating polarizer and data acquisition device which, as stated, makes measurements easier, faster and more precise than manual operation.

Depending on the level of students, many aspects of the experiment may be partially or fully completed for them, to tailor the learning to their skill set. For instance, if they are not expected to be able to perform non-linear fits, they could be provided with the Malus' law fitting algorithm. In particular, the full process of calibrating the magnetic field, as set out in Appendix A, was fairly advanced and for students it should be sufficient to determine B_{oil} at each magnet separation simply by taking an average of several measurements. The full calibration then presents an interesting area in which students can extend the experiment. Other avenues for extension include attempting to use the Verdet coefficient to detect adulteration of olive oil (similar to another experiment in the literature [30]) or measuring the Verdet coefficient of other fluids.

6. Conclusions

We have devised a simple experimental procedure based on Malus' law which measures polarization rotations with a precision of up to 50 μrads. The versatility of the Malus' law fitting method allows it to be used in a variety of different polarimetry experiments including the study of chirality in sugars, stress-induced birefringence in plastics and magneto-induced birefringence in liquids and gases. To prove the efficacy of our method, we studied the Faraday effect in olive oil and were able to measure Verdet coefficients with errors as small as 0.4%. Our results agree well with values in the literature and we present excellent fits to dispersive models. The experiment is simple in its execution and equipment, yet can provide profound insight into fundamental concepts in optics and electromagnetism and as such is well-suited to being used as an undergraduate teaching experiment. The experiment provides training in a wide range of experimental skills, including data analysis and error analysis. In addition,

the versatility of the apparatus provides ample opportunity for extension.

Acknowledgements

We would like to thank Dr Aidan Hindmarch and Dr Jason Anderson for providing data aquisition software, Chloe So for help and advice, Durham University for providing the equipment and funding required to complete this investigation and the reviewers for their time and helpful input.

NLRS and CSA acknowledge financial support from EPSRC Grant Ref. No. EP/M014398/1. IGH and CSA acknowledge financial support from EPSRC Grant Ref. No. EP/R002061/1. The data in this paper are available from [31]

References

[1] Adams C S and Hughes I G 2019 *Optics f2f* (Oxford: Oxford University Press) ch 4
[2] Öhman Y 1956 *Stockholm Obs. Ann.* **19** (11) 3
[3] Dick D J and Shay T M 1991 *Optics Letters* **16** 867
[4] Weller L, Kleinbach K S, Zentile M A, Knappe S, Hughes I G and Adams C S 2012 *Optics Letters* **37** (16) 3405
[5] Gardner F F and Whiteoak J B 1963 *Nature* **197** 1162
[6] Massachusetts Institute of Technology Physics Department *The Faraday Effect* {http://web.mit.edu/8.13/www/JLExperiments/JLExp08.pdf} [Accessed 31st July 2019]
[7] Rutgers University Physics Department *The Faraday Effect* {http://www.physics.rutgers.edu/~eandrei/389/faraday.pdf} [Accessed 31st July 2019]
[8] Compton R N and Duncan M A 2016 *Laser Experiments for Chemistry and Physics* (Oxford: Oxford University Press) ch 20
[9] Mahurin S M, Compton R N and Zare R N 1999 *J. Chem. Edu.* **76** 1234
[10] Nixon M and Hughes I G 2017 *Eur. J. Phys.* **38** 045302
[11] Loeffler F J 1983 *Am. J. Phys.* **51** 661
[12] Pedrotti F L and Bandettini P 1990 *Am. J. Phys.* **58** 542
[13] Hunte C 2018 *Eur. J. Phys.* **39** 025301
[14] Jacob D, Vallet M, Bretenaker F, Le Floch A and Le Naour R 1995 *Appl. Phys. Lett.* **66** 3546
[15] Van Baak D A 1996 *Am. J. Phys.* **64** 724
[16] Jain A, Kumar J, Zhou F, Li L and Tripathy S 1999 *Am. J. Phys.* **67** 714
[17] Valev V K, Wouters J and Verbiest T 2008 *Eur. J. Phys.* **29** 1099
[18] Valev V K, Wouters J and Verbiest T 2008 *Am. J. Phys.* **76** 626
[19] Phelps G, Abney J., Broering M. and Korsch W. 2015 *Rev. Sci. Instrum.* **86** 073107
[20] Chang C, Wang L, Shy J, Lin C and Chou C 2011 *Rev. Sci. Instrum.* **82** 063112
[21] Brandon W, Mandjiny S, McDonald K and Lee D 2017 *European Scientific Journal* October 2017 Special Edition 111
[22] Duffy R M and Netterfield R P 1983 *Applied Optics* **22** (9) 1272
[23] Shakir A A, AL-Mudhafa R D and Anwaar A A 2013 *J. Adv. EEE* **2** (3) 362
[24] Cauchy A L 1830 *Bull. Sci. Math.* **14** 6
[25] Cauchy A L 1836 *Mémoire sur la Dispersion de la Lumière* (Prague: Calve)
[26] Drude P 1900 *Lehrbuch der Optik 1st Ed.* (Leipzig: S. Hirzel)
[27] So C, Spong N L R, Möhl C, Jiao Y and Adams C S Zeeman-tunable Modulation Transfer Spectroscopy arXiv:1906.04154
[28] Hughes I G and Hase T P A 2010 *Measurements and their Uncertainties* (Oxford: Oxford University Press) ch 9
[29] Teach Spin *Faraday Rotation* {https://www.teachspin.com/faraday-rotation} [Accessed 14th September 2019]
[30] Abu-Taha M I, Halasa M A and Abu-Samreh M M 2012 *Journal of Modern Physics* **4** 230
[31] Durham University Collections {http://doi.org/10.15128/r2ng451h53g}
[32] Weller L 2013 *PhD Thesis* Durham University Appendix F. Available at Durham E-Theses Online: {http://etheses.dur.ac.uk/7747/}
[33] Ramaseshan S 1946 *Proc. Indian Acad. Sci.* **A24** 426

Appendix A. Magnetic field modelling

As described previously, the magnetic field was provided by a pair of annular neodymium permanent magnets. The magnets were N52 grade, with a NiCuNi coating and were produced bespoke according to our mechanical drawings (see supplementary material) by Jinmagnets Industrial Co. (http://www.jinmagnets.com). Whilst we chose to use custom-produced magnets, any strong annular or ring-like magnet (which are common and cheap) would be suitable.

To hold the magnets in place we machined custom magnet fittings and custom holders. The cylindrical magnet fittings were machined from brass and threaded. The holders were machined from aluminium and similarly threaded allowing the fittings to screw in and making it simple to alter the magnet separation; we machined brass handles for the fittings to make the screwing easier. The magnet holders were kept apart by aluminium separators at the top and bottom. For full technical drawings of the magnets and our custom mount, please see the supplementary material.

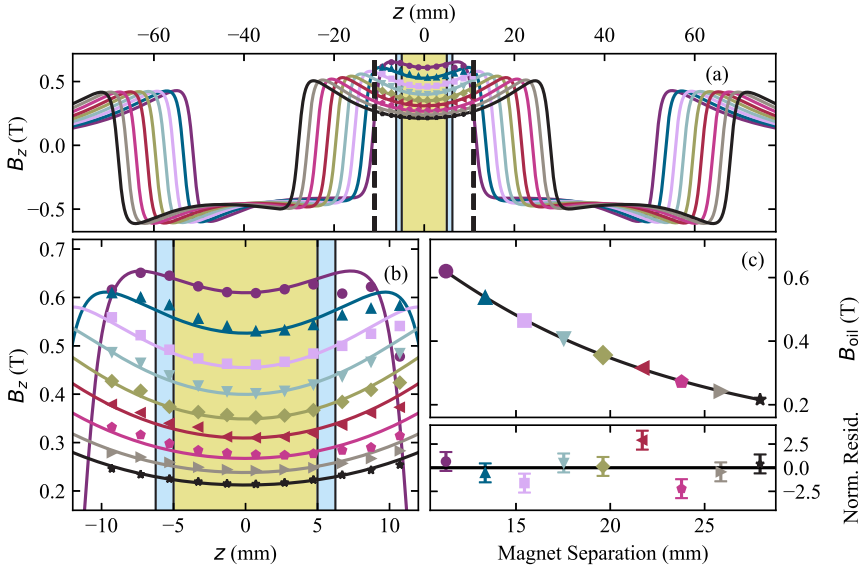

Figure A1. (a) The spatial homogeneity of the magnetic field along the z direction for each separation distance. The point $z = 0$ represents the position equidistant from the magnets, at which the centre of the sample is placed. The theory curves are fitted according to (A.1) The dotted lines show the minimum separation of the magnets i.e. the spatial region in which data were collected. (b) A zoomed-in plot of the region between the dotted lines of the upper figure. This plot shows the effect of altering the magnet separation on the field strength in the region between the magnets. The outer shaded region shows the position of the glass walls of the cuvette ($l_{\text{glass}} = 2.48 \pm 0.01$ mm) and the inner shaded region shows the position of the oil ($l_{\text{oil}} = 10.00 \pm 0.01$ mm). (c) The variation of the average magnetic field strength in the oil (B_{oil}) as a function of the magnet separation. The lower plot displays the normalized residuals. (color online).

The magnetic field was calibrated to determine the spatial homogeneity and average field strength at each magnet separation distance. Each full rotation of

the magnets in their mount increased their separation by approximately 2 mm and therefore reduced the magnetic field.

The spatial homogeneity was measured using a transverse Hall probe which was moved along the direction of laser propagation through the magnetic field (z axis). These measurements are summarized in figure A1(a) and (b). Theory curves were fit to the data by considering the axial field strength B_z at a distance z from a cylindrical magnet with uniform magnetization B_0 and radius R:

$$B_z = \frac{B_0}{2}\left[\frac{z+z_0+t}{\sqrt{(z+z_0+t)^2+R^2}} - \frac{z+z_0-t}{\sqrt{(z+z_0-t)^2+R^2}}\right] \tag{A.1}$$

where z_0 is an offset to account for the fact that the magnet is not at the origin and t is the thickness of the magnet (for more detail see [32]). As seen in figure 1(b), the magnets were not perfect cylinders and so the field produced by the magnet was determined by piecewise addition of the field due to each part of the magnet and a subtraction due to the hole bored through the magnet's centre. It was then possible to sum the contributions from each magnet to work out the overall field strength at each z position.

The theory curves were used to calculate the average field strength experienced by the oil (B_{oil}) for each separation distance; these results are summarized in figure A1(c). It should be noted that the average field strength experienced by the combined sample (B_{combined}) and cuvette (B_{cuvette}) are not the same as for the oil alone. However, as shown by (8), B_{oil} is the only field strength required to calculate the Verdet coefficient of the oil.

Appendix B. Verdet coefficients in glass

As discussed in the results section, to determine the Verdet coefficient for olive oil it was necessary to perform a separate set of measurements with an empty cuvette to subtract the rotation induced by the glass. A side-effect of performing these measurements is that we were able to determine Verdet coefficients for the UV fused quartz glass at each of the wavelengths we tested; these are summarized in table B1. In general, the glass Verdet coefficients have a larger uncertainty than those for the oil, this could be due to the shorter path length of the glass.

Figure B1 shows the dispersion curves applied to our data for the glass. As with the olive oil data, the dispersive models fit well and our data is in good agreement with the literature [33]. The exception is the data point corresponding to 796.2 nm

Table B1. The determined Verdet coefficients for the UV fused quartz glass cuvette at approximately 20 °C.

Wavelength ± 0.1 (nm)	Verdet coefficient (deg T^{-1} m^{-1})
405.4	540 ± 16
446.6	431 ± 5
518.8	293 ± 13
637.8	196 ± 11
659.2	181 ± 2
681.8	190 ± 30
796.2	370 ± 50

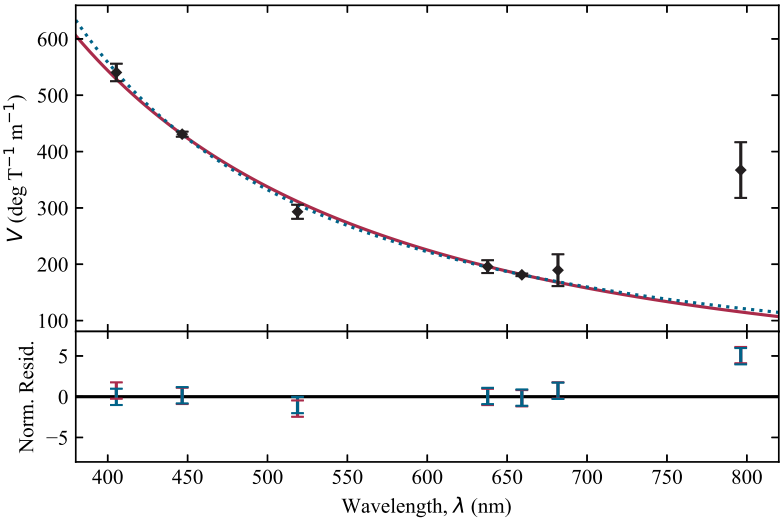

Figure B1. Dispersion plot for the variation of the Verdet coefficient of quartz glass with wavelength at approximately 20 °C. The data are represented by black diamonds with their error bars in the y direction displayed (error bars in x are too small to be seen). The solid red line represents the Cauchy-type model described by $V = A + B/\lambda^2$ and the dotted blue line represents the Drude-type model described by $V = A/(\lambda^2 - \lambda_0^2)$. The χ^2_ν values for these models are 5.86 and 5.26 respectively. The lower plot displays the normalized residuals. The point corresponding to 796.2 nm does not fit the model well and has a very large error; this could be due to incomplete extinction of the polarizers or a separate absorption peak in the IR region.

which is far from the models and has a large error. We believe this may be due to the polarizers being unsuited to the near-IR region. Alternatively, the quartz glass may possess an absorption peak in the IR region, such that this wavelength is actually part of a separate dispersion curve - though this would require further study to confirm. Whilst we focused on the Faraday effect in olive oil, we show here that our method may be used more generally and also works well for the Faraday effect in solids.